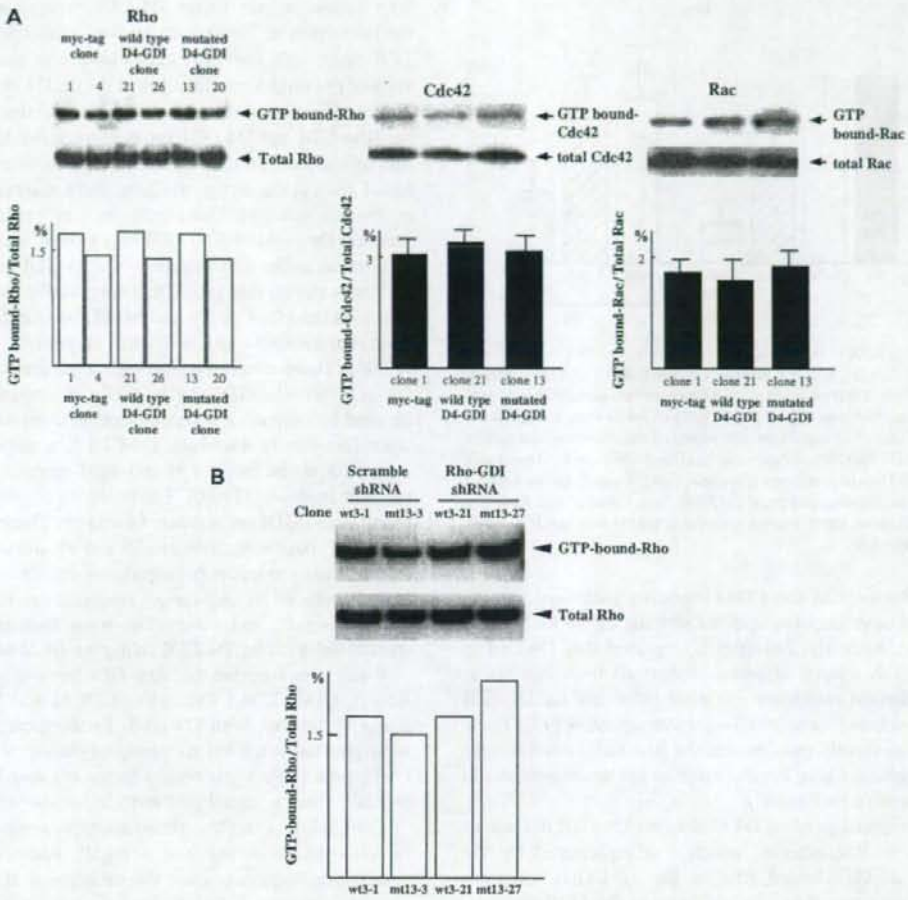

Figure 9. Detection of cellular guanine triphosphate (GTP)–bound Rho and Rac in leukemic cells. (**A**) Cells lysates were clarified by centrifugation, and equal volumes of lysates were incubated with 20 μg glutathione S-transferase (GST)–Rho-binding domain (RBD) beads. Beads were washed four times. Bound Rho proteins were detected by Western blotting using an anti-RhoA monoclonal antibody. The upper figures show the expressions of GTP-bound Rho and total Rho in all clones. The amounts of activated Rho (GTP-bound form) in all clones were almost the same. In order to quantitate the amount of GTP-bound Rho, a densitometric analysis was performed using NIH image version 1.62. The amount of RBD-bound Rho was normalized to the total amount of Rho in cell lysates for comparison of Rho activities (level of GTP-bound Rho) among different samples. The ratios of GTP-bound Rho to total Rho are shown in the lower graph. The GTP-bound Rho accounted for 1.3% to 1.6 % of total Rho in these six clones. There are no significant differences among the clones. The measurement of Rac activity was performed using the Rac Activation Assay kit (Cytoskeleton, Denver, CO, USA) according to the manufacturer's protocol. Amounts of activated Rac (GTP-bound form) in three clones were almost similar. In order to quantitate the amount of GTP-bound forms, a densitometric analysis was performed. The amount of GTP-bound Rac was normalized to the total amount of Rac in cell lysates for comparison of Rac activities among different samples. The ratios of GTP-bound Rac to total Rac are shown in the lower graph. The GTP- bound Rac accounted for 1.7% to 1.9% of total Rac in three clones, respectively. There are no significant differences among the clones. (**B**) Alterations of cellular GTP-bound Rho under the condition of decreased expression of Rho-GDI in leukemic cells with wt D4-GDI or mt D4-GDI overexpression. The pull-down assay for Rho using the wild-type or mutated D4-GDI clones (wt3-1, wt3-21, mt13-3, or mt3-27) with a vector of scramble shRNA or a vector for shRNA of Rho-GDI were done. As a result, the GTP-bound Rho in Rho-GDI knockdown mt D4 clones (mt13-27) was slightly increased compared with clones with scramble shRNA vector (wt3-1 and mt13-3) or Rho-GDI knockdown wt D4 clones (wt3-21).

cell lung carcinoma cells [40]. We reported that Rho activation augmented leukemic cell invasion through acceleration of cell adhesion, but not cell proliferation [1]. Itoh et al. [41] indicated rho-associated kinase played an essential part in tumor cell invasion, and that rho-associated kinase inhibitor may have potential as a therapy for prevention of malignant invasion and metastasis. In addition, Rho-GDI may also play a role in cancer invasion and metastasis

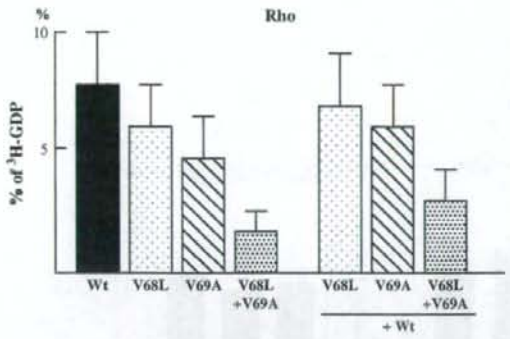

Figure 10. [^{3}H]GDP dissociation assay of Rho. The inhibitory activities of mutated (mt) D4 with two mutations of V68L and V69A on the dissociation of [^{3}H]GDP from isoprenylated Rho were less active than wild-type (wt) D4. The decreased dissociation activity of D4 with each single mutation (V68L orV69A) was slight. The results of the inhibitory activities of wt plus mt D4 with both mutations of V68L and V69A on the dissociation of [^{3}H]GDP from isoprenylated Rho showed mt D4 was dominant negative of wt D4 on the dissociation of [^{3}H]GDP from isoprenylated Rho. The dominant negative effect was not observed in the D4 with single mutation of V68L orV69A.

via involvement in the CD44 signaling pathway, because Rho-GDI coimmunoprecipitated with the CD44-ERM complex [42]. Recently, Zhang et al. reported that D4-GDI is expressed in a panel of breast cancer cell lines, but not in benign-derived mammary epithelial cells, and the D4-GDI modulates breast cancer cell–invasive activities [43]. These findings obviously indicate that the Rho family and its regulatory proteins play critical roles in the development and progression of malignancy.

Overexpression of wt D4-GDI or mt D4-GDI did not alter Rho or Rac activity, which was represented by the amount of GTP-bound Rho or Rac. D4-GDI functions both to inactivate Rho, via inhibition of the GDP dissociation from Rho, and to activate Rho, via suppression of the GTPase activity of Rho itself. Furthermore, D4-GDI has weaker GDP dissociation inhibitory activity (10-fold less) than Rho-GDI. Recently, Zhang et al. [43] reported that the activation status of Rac1, Cdc42, and RhoA was not altered as a result of D4-GDI depletion. In addition, like other Rho-GDIs, D4-GDI was postulated to bind and inhibit Rho GTPases. However, much yet remains to characterize the specificity of D4-GDI [15,16]. Although recombinant D4-GDI binds to purified Rac1, Cdc42, and RhoA, there is no evidence showing that they can form stable complexes in vivo [43]. Thus, the lack of changes in Rho or Rac activity in response to exogenous expression of wt D4-GDI or mt D4-GDI may be explained. On the other hand, the GTP-bound Rho in mt D4-GDI clone with Rho-GDI was slightly increased in contrast to mt D4-GDI clone without Rho-GDI knockdown or wt D4-GDI clones with/without Rho-GDI knockdown. These results suggest that the altered phenotypes of leukemic cells may be partially caused by Rho activation due to mt D4-GDI expression. However, the invasiveness, motility, and adhesion activity of mt D4-GDI clone with Rho-GDI knockdown was not changed in spite of the mild Rho activation in the mt D4 clone. Ishizaki et al. [44] recently report that combined disruption of both the Rho-GDI and D4-GDI genes in mice resulted in reduction of marginal zone B cells in the spleen, retention of mature T cells in the thymic medulla, and a marked increase in eosinophil numbers. Our results may be explained by the fact that the level of Rho-GDI knockdown was insufficient in contrast to the null mutation of Rho-GDI gene.

It was shown that D4-GDI is specifically cleaved at two positions (residues 18–19 and 54–55) by two different apoptosis proteases, caspase-3 and caspase-1, respectively [17,45]. These consensus cleavage sequences are not present in either Rho-GDI or Rho-GDIγ. A truncated D4-GDI cleaved by caspase-1 is unable to effectively bind and regulate Rho family members. D4-GDI is a target protein of caspase-3 in the process of anti–IgM-mediated or Fas-dependent apoptosis [17,46]. The positions of point mutations found in D4-GDI are residues 68 and 69. Therefore, the positions of these mutations are 13 and 49 amino acids from the cleavage sequence. No significant differences in the apoptosis induced by anti-cancer reagents, i.e., methotrexate, cyclohexamide, and vincristine, were seen in Raji cells transferred with mt D4-GDI transgene (data not shown).

It has been reported that Rho-GDI forms a complex with Rho A, CDC42, and Rac, while CDC42 and Rac was not found to interact with D4-GDI. Furthermore, stimulation with phorbol ester led to phosphorylation of D4-GDI in U937 cells [15]. Their results suggested that D4-GDI can regulate specific signal pathways in hematopoietic cells.

D4-GDI is a highly abundant cytoplasmic protein in lymphocytes, and has had a highly conserved primary amino acid sequence since the divergence of mammalian species. However, D4-GDI–deficient mice and in vitro embryonal stem cell differentiation analysis indicated D4-GDI expression is not essential for hematopoiesis and did not clarify its function in hematopoietic cells [47,48]. Our results indicate that D4-GDI overexpression in transformed cells changes cell motility, cell adhesion, and invasiveness in some organs. In normal lymphocytes, D4-GDI may have a subtle, yet crucial, function related to cell motility and adhesion.

Li et al. [49] reported that D4-GDI might be involved in the progression of human cutaneous T-cell lymphoma using a cDNA microarray in the clonally related T-cell lines derived from different stages of a progressive T-cell lymphoma involving skin. They found the D4-GDI gene to be one of the downregulated genes in cells from an advanced, clinically aggressive stage lymphoma, in contrast to cells from an earlier, clinically indolent stage of lymphoma. Expression of D4-GDI mRNA in cells derived from the aggressive stage lymphoma was shown to be markedly decreased as compared with cells derived from

the earlier-stage lymphoma. This result is compatible with our data, showing overexpression of wt D4-GDI to reduce the invasiveness of human leukemic cells. Thus, D4-GDI may assure the progression and invasion of human leukemia through its mutations and/or its downregulation.

Accumulating recent evidence shows that D4-GDI is expressed not only in hematopoietic tissues, but also in nonhematopoietic neoplasms. Results of cDNA microarray analyses revealed that D4-GDI is upregulated in ovarian [50], and downregulated in bladder, carcinomas [51]. On the other hand, Theodorescu et al. [52] found that D4-GDI protein expression in bladder tumors is reduced as a function of bladder tumor progression. This result has suggested that D4-GDI is a metastasis suppressor gene in models of bladder cancer. In contrast, the results of Zhang et al. [43] show that increased expression of D4-GDI promotes cell invasiveness in breast cancer cells. These results suggest that the D4-GDI may have certain roles in the progression of different types of cancer. Thus, it is reasonable to propose that D4-GDI may be involved more generally in the invasive phenotype of human cancer.

Acknowledgments

We thank Dr. Martin Alexander Schwartz (The Scripps Research Institute, La Jolla, C, USA) for generously providing a expression vector of GST-RBD. We thank Ms. Megumi Takamatsu, Mrs. Michiko Takahashi, and Dr. Yan Xiu, for cell culture and animal care, Mr. Hiroshi Suzuki for immunohistochemistry and Mr. Kohji Takeichi for technical photographic support.

This work was supported by Grants-in Aid for Pediatric Research (9C-5, 12C-1) from the Ministry of Health and Welfare, a research grant from the Ministry of Education in Japan (05404022, 07670258, 07770163, 1770124, 11670193, 10307004), National Grant-in-Aid for the Establishment of a High-Tech Research Center in a Private University, Sankyo Foundation of Life Science, Tsumura Foundation for Medical Research, Kawano Foundation for Children Cancer Research, and Keio Gijuku Academic Development Funds and a special grant-in-aid for innovative and collaborative research projects at Keio University.

References

1. Fukushima S, Yamada T, Hashiguchi A, Nakata Y, Hata J. Augmentation of human leukemia cell invasion by the activation of small GTP-binding protein Rho. Exp Hematol. 2000;28:391–400.
2. Hall A. Small GTP-binding proteins and the regulation of the actin cytoskeleton. Annu Rev Cell Biol. 1994;10:31–54.
3. Takai Y, Sasaki T, Tanaka K, Nakanishi H. Rho as a regulator of the cytoskeleton. Trends Biochem Sci. 1995;20:227–231.
4. Narumiya S. The small GTPase Rho: cellular functions and signal transduction. J Biochem. 1996;120:215–228.
5. Hall A. Rho GTPases and the actin cytoskeleton. Science. 1998;279: 509–514.
6. Vojtek AB, Cooper JA. Rho family members: activators of MAP kinase cascades. Cell. 1995;82:527–529.
7. Van Aelst L, D'Souza-Schorey C. Rho GTPases and signaling networks. Genes Dev. 1997;11:2295–2322.
8. Lelias JM, Adra CN, Wulf GM, et al. cDNA cloning of a human mRNA preferentially expressed in hematopoietic cells and with homology to a GDP-dissociation inhibitor for the rho GTP-binding proteins. Proc Natl Acad Sci U S A. 1993;90:1479–1483.
9. Scherle P, Behrens T, Staudt LM. Ly-GDI, a GDP-dissociation inhibitor of the RhoA GTP-binding protein, is expressed preferentially in lymphocytes. Proc Natl Acad Sci U S A. 1993;90:7568–7572.
10. Adra CN, Manor D, Ko JL, et al. Rho-GDIγ: a GDP-dissociation inhibitor for Rho proteins with preferential expression in brain and pancreas. Proc Natl Acad Sci U S A. 1997;94:4279–4284.
11. DerMardirossian C, Bokoch GM. GDIs: central regulatory molecules in Rho GTPase activation. Trends Cell Biol. 2005;15:356–363.
12. Hart MJ, Maru Y, Leonard D, Witte ON, Evans T, Cerione RA. A GDP dissociation inhibitor that serves as a GTPase inhibitor for the Ras-like protein CDC42Hs. Science. 1992;258:812–815.
13. Chuang TH, Xu X, Knaus UG, Hart MJ, Bokoch GM. GDP dissociation inhibitor prevents intrinsic and GTPase activating protein-stimulated GTP hydrolysis by the Rac GTP-binding protein. J Biol Chem. 1993;268:775–778.
14. Takahashi K, Sasaki T, Mammoto A, et al. Direct interaction of the Rho GDP dissociation inhibitor with ezrin/radixin/moesin initiates the activation of the Rho small G protein. J Biol Chem. 1997;272. 23371–22375.
15. Gorvel JP, Chang TC, Boretto J, et al. Differential properties of D4/LyGDI versus RhoGDI: phosphorylation and rho GTPase selectivity. FEBS Lett. 1998;422:269–273.
16. Golovanov AP, Chuang TH, DerMardirossian C, et al. Structure-activity relationships in flexible protein domains: regulation of rho GTPases by RhoGDI and D4 GDI. J Mol Biol. 2001;305:121–135.
17. Na S, Chuang TH, Cunningham A, et al. D4-GDI, a substrate of CPP32, is proteolyzed during Fas-induced apoptosis. J Biol Chem. 1996;271:11209–11213.
18. Krieser RJ, Eastman A. Cleavage and nuclear translocation of the caspase 3 substrate Rho GDP-dissociation inhibitor, D4-GDI, during apoptosis. Cell Death Differ. 1999;6:412–419.
19. Bos JL. Ras oncogenes in human cancer: a review. Cancer Res. 1989; 49:4682–4689.
20. Moscow JA, He R, Gnarra JR, et al. Examination of human tumors for rhoA mutations. Oncogene. 1994;9:189–194.
21. Boivin D, Bilodeau D, Beliveau R. Regulation of cytoskeletal functions by Rho small GTP-binding proteins in normal and cancer cells. Can J Physiol Pharmacol. 1996;74:801–810.
22. Crespo P, Schuebel KE, Ostrom AA, Gutkind JS, Bustelo XR. Phosphotyrosine-dependent activation of Rac-1 GDP/GTP exchange by the vav proto-oncogene product. Nature. 1997;385:169–172.
23. Eva A, Aaronson SA. Isolation of a new human oncogene from a diffuse B-cell lymphoma. Nature. 1985;316:273–275.
24. Habets GG, Scholtes EH, Zuydgeest D, et al. Identification of an invasion-inducing gene, Tiam-1, that encodes a protein with homology to GDP-GTP exchangers for Rho-like proteins. Cell. 1994;77:537–549.
25. Aznar S, Fernandez-Valeron P, Espina C, et al. Rho GTPases: potential candidates for anticancer therapy. Cancer Lett. 2004;206:181–191.
26. Banyard J, Anand-Apte B, Symons M, et al. Motility and invasion are differentially modulated by Rho family GTPases. Oncogene. 2000;19: 580–591.
27. Jaffe AB, Hall A. Rho GTPases in transformation and metastasis. Adv Cancer Res. 2002;84:57–80.
28. Lin M, van Golen KL. Rho-regulatory proteins in breast cancer cell motility and invasion. Breast Cancer Res Treat. 2004;84:49–60.
29. Rosenfeld C, Goutner A, Choquet C, et al. Phenotypic characterisation of a unique non-T, non-B acute lymphoblastic leukaemia cell line. Nature. 1977;267:841–843.
30. Uphoff CC, MacLeod RA, Denkmann SA, et al. Occurrence of TEL-AML1 fusion resulting from (12;21) translocation in human early B-lineage leukemia cell lines. Leukemia. 1997;11:441–447.

31. Morikawa S, Tatsumi E, Baba M, Harada T, Yasuhira K. Two E-rosette-forming lymphoid cell lines. Int J Cancer. 1978;21:166–170.
32. Sambrook J, Fritsch EF, Maniatis T. Molecular Cloning: A Laboratory Manual. 2nd ed. New York: Cold Spring Harbor Laboratory Press; 1989.
33. Hall PA, Levison DA, Woods AL, et al. Proliferating cell nuclear antigen (PCNA) immunolocalization in paraffin sections: an index of cell proliferation with evidence of deregulated expression in some neoplasms. J Pathol. 1990;162:285–294.
34. Ren XD, Kiosses WB, Schwartz MA. Regulation of the small GTP-binding protein Rho by cell adhesion and the cytoskeleton. EMBO J. 1999;18:578–585.
35. Reid T, Furuyashiki T, Ishizaki T, et al. Rhotekin, a putative target for Rho bearing homology to a serine/threonine kinase, PKN and Rhophilin in the Rho binding domain. J Biol Chem. 1996;271: 13556–13560.
36. Gosser YQ, Nomanbhoy TK, Aghazadeh B, et al. C-terminal binding domain of Rho GDP-dissociation inhibitor directs N-terminal inhibitory peptide to GTPases. Nature. 1997;387:814–819.
37. Biou V, Gibrat JF, Levin JM, Robson B, Garnier J. Secondary structure prediction: combination of three different methods. Protein Eng. 1988; 2:185–191.
38. Hordijk PL, ten Klooster JP, Van der Kammen RA, Michiels F, Oomen LCJM, Collard JG. Inhibition of invasion of epithelial cells by Tiam1-Rac signaling. Science. 1997;278:1464–1466.
39. Hotchin NA, Hall A. The assembly of integrin adhesion complexes requires both extracellular matrix and intracellular rho/rac GTPases. J Cell Biol. 1995;131:1857–1865.
40. Tokman MG, Porter RA, Williams CL. Regulation of cadherin-mediated adhesion by the small GTP-binding protein Rho in small cell lung carcinoma cells. Cancer Res. 1997;57:1785–1793.
41. Itoh K, Yoshioka K, Akedo H, Uehata M, Ishizaki T, Narumiya S. An essential part Rho-associated kinase in the transcellular invasion of tumor cells. Nat Med. 1999;5:221–225.
42. Hirao M, Sato N, Kondo T, et al. Regulation mechanism of ERM (ezrin/radixin/moesin) protein/plasma membrane association: possible involvement of phosphatidylinositol turnover and Rho-dependent signaling pathway. J Cell Biol. 1996;135:37–51.
43. Zhang Y, Zhang B. D4-GDI, a Rho GTPase regulator, promotes breast cancer cell invasiveness. Cancer Res. 2006;66:5592–5598.
44. Ishizaki H, Togawa A, Tanaka-Okamoto M, et al. Defective chemokine-directed lymphocyte migration and development in the absence of rho guanosine diphosphate-dissociation inhibitors alpha and beta. J Immunol. 2006;177:8512–8521.
45. Danley DE, Chuang TH, Bokoch GM. Defective Rho GTPase regulation by IL-1 beta-converting enzyme-mediated cleavage of D4 GDP dissociation inhibitor. J Immunol. 1996;157:500–503.
46. Rickers A, Brockstedt E, Mapara MY, Otto A, Dorken B, Bommert K. Inhibition of CPP32 blocks surface IgM-mediated apoptosis and D4-GDI cleavage in human BL60 Burkitt lymphoma cells. Eur J Immunol. 1998;28:296–304.
47. Yin L, Schwartzberg P, Scharton-Kersten TM, Staudt L, Lenardo M. Immune responses in mice deficient in Ly-GDI, a lymphoid-specific regulator of Rho GTPases. Mol Immunol. 1997;34:481–491.
48. Guillemot J-C, Kruskal BA, Adra CN, et al. Targeted disruption of guanosine diiphosphate-dissociation inhibitor for Rho-related protein, GDID4: normal hematopoietic differentiation but subtle defect in superoxide production by macrophages derived from in vitro embryonal stem cell differentiation. Blood. 1996;88:2722–2731.
49. Li S, Ross DT, Kadin ME, Brown PO, Wasik MA. Comparative genome-scale analysis of gene expression profiles in t cell lymphoma cells during malignant progression using a complementary DNA microarray. Am J Pathol. 2001;158:1231–1237.
50. Tapper J, Kettunen E, El Rifai W, et al. Changes in gene expression during progression of ovarian carcinoma. Cancer Genet Cytogenet. 2001;128:1–6.
51. Gildea JJ, Seraj MJ, Oxford G, et al. RhoGDI2 is an invasion and metastasis suppressor gene in human cancer. Cancer Res. 2002;62:6418–6423.
52. Theodorescu D, Sapinoso LM, Conaway MR, et al. Reduced expression of metastasis suppressor RhoGDI2 is associated with decreased survival for patients with bladder cancer. Clin Cancer Res. 2004;10: 3800–3806.

Leukemia & Lymphoma, April 2008; 49(4): 757–762

informa
healthcare

ORIGINAL ARTICLE: CLINICAL

Outcome of childhood B-cell non-Hodgkin lymphoma and B-cell acute lymphoblastic leukemia treated with the Tokyo Children's Cancer Study Group NHL B9604 protocol

AKIRA KIKUCHI[1], TETSUYA MORI[2], JUN-ICHIRO FUJIMOTO[3], MASAAKI KUMAGAI[4], SHOSUKE SUNAMI[5], YURI OKIMOTO[6], & MASAHIRO TSUCHIDA[7]

[1]*Division of Hematology/Oncology, Saitama Children's Medical Center, Saitama-shi Saitama 339-8551, Japan,* [2]*Department of Pediatric Oncology, National Center for Child Health and Development, Tokyo, Japan,* [3]*National Research Institute for Child Health and Development, Tokyo, Japan,* [4]*Department of Hematology, National Center for Child Health and Development, Tokyo, Japan,* [5]*Department of Pediatrics, Japanese Red Cross Narita Hospital, Chiba, Japan,* [6]*Department of Hematology–Oncology, Chiba Children's Hospital, Chiba, Japan, and* [7]*Department of Pediatrics, Ibaraki Children's Hospital, Ibaraki, Japan*

(Received 10 September 2007; revised 30 November 2007; accepted 3 December 2007)

Abstract

From June 1996 to January 2001, 91 patients with B-cell non-Hodgkin lymphoma or B-cell acute lymphoblastic leukemia up to 18 years of age were enrolled in Tokyo Children's Cancer Study Group (TCCSG) NHL B9604 protocol study. Five-day intensive chemotherapy courses including high-dose methotrexate and high-dose cyclophosphamide were used for localized disease (Groups A and B). High-dose cytarabine was added for advanced disease (Groups C and D). Fifteen patients experienced an adverse event. There were three induction failures, eight relapses (three local, four bone marrow (BM), one BM + local), two toxic deaths and two second malignant neoplasm. Event-free survival at 6 years in Group D and in all patients was 82.4% ± 9.2% and 81.9% ± 4.4%, respectively. The TCCSG NHL B9604 protocol achieved an excellent treatment outcome especially in patients with the most advanced disease (Group D: high BM blast cell burden and/or central nervous system involvement).

Keywords: *B-NHL, B-ALL, intensified chemotherapy, TCCSG NHL B9604*

Introduction

The malignant cells of B-cell (surface immunoglobulin-positive [Ig+]) non-Hodgkin lymphoma (B-NHL) and B-cell acute lymphoblastic leukemia (B-ALL), which are classified as Burkitt lymphoma/leukemia in WHO classification [1], share morphologic, immunophenotypic, cytogenetic and clinical features and are considered to represent a continuum of the same disease. Diffuse large B-cell lymphoma is a distinct disease entity from Burkitt lymphoma/leukemia. However, the treatment for patients with large cell lymphoma is the same as that for patients with Burkitt histology. In early trials, children with advanced B-NHL and B-ALL had a worse outcome characterized by early recurrences despite a high initial complete remission rate [2,3]. After the introduction of short, intensive therapy courses primarily based on cyclophosphamide (CY), methotrexate (MTX), and intrathecal (i.t.) therapy, the prognosis of these mature B-cell neoplasms has improved significantly [4–11].

Most previous clinical experiences about childhood B-NHL and B-ALL were reported from European and North American study groups, however, there are few data on Japanese or Asian patients. We report here the treatment and results of 91 Japanese children with B-NHL or B-ALL registered to the Tokyo Children's Cancer Study Group (TCCSG) NHL B9604. The aim of this study

Correspondence: Akira Kikuchi MD, Division of Hematology/Oncology, Saitama Children's Medical Center, 2100 Magome Iwatsuki-ku, Saitama-shi Saitama 339-8551, Japan. Tel: +81-48-7581811. Fax: +81-48-7581818. E-mail: a1091069@pref.saitama.lg.jp

ISSN 1042-8194 print/ISSN 1029-2403 online © 2008 Informa UK Ltd.
DOI: 10.1080/10428190701843239

was to evaluate the efficacy and safety of the short and intensive chemotherapy regimen designed by TCCSG for childhood B-NHL or B-ALL.

Patients and methods

Children and adolescents up to 18 years of age newly diagnosed with B-NHL or B-ALL were eligible for this study. From June 1996 to January 2001, 91 patients with B-NHL or B-ALL were enrolled in this study. Diagnosis was made by pathologists at a regional hospital and registration was made based on the regional diagnosis. A central review was performed retrospectively by the reference laboratory according to the WHO classification [1]. The St. Jude system was used for disease staging [12]. Patients were stratified into four groups according to stage, resection status, bone marrow (BM) blast cell burden and central nervous system (CNS) involvement as shown in Figure 1.

Five-day intensive chemotherapy courses including high-dose MTX (HD-MTX) and high-dose CY (HD-CY) were used for Groups A and B. High-dose cytarabine (HD-AraC) was added for Groups C and D. Patients in Groups B, C and D received a 5-day cytoreductive prephase before the first course was administered (Table I). Courses were administered at 3–4-week intervals. The number of treatment courses was three in Group A, six in B, six in C and seven in D, respectively. Treatment duration ranged from 10 to 27 weeks (Figure 1).

Events were defined as induction failure, relapse, death in induction, death in remission and second malignant neoplasm. Survival curves were calculated by the Kaplan–Meier method. Toxicities were graded according to National Cancer Institute Common Toxicity Criteria version 2. All treatments were performed with informed consent from the patients' guardians.

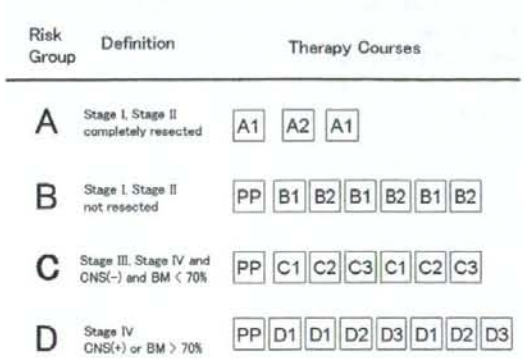

Figure 1. Treatment strategy. Patients were stratified into four risk groups; A, B, C and D. The composition of therapy courses is shown in Table I.

Results

The clinical characteristics of the 91 patients are shown in Table II. The percentage in Group A patients in our series was quite small (3.3%) compared with that of equal disease status patients in other studies (7–17%) [6,8,11]. A retrospective central review was performed in 64.8% (59/91) of the enrolled patients and the concordance rate was 88.1% (52/59). Fifteen patients experienced an adverse event. There were three induction failures, eight relapses (three local, four BM, one BM + local), two toxic deaths and two second malignant neoplasm. Nine patients died of induction failure in three, relapse in four and toxicity in two patients [intracranial hemorrhage (ICH) and sepsis]. Two patients developed a second malignant neoplasm. Grade 4 non-hematological toxicity was noted in 4 cases. Event-free survival (EFS) and overall survival (OS) were calculated as follows: EFS and OS in total were 81.9% ± 4.4% and 90.1% ± 3.1%, respectively. EFS was 66.7% ± 27.2% in Group A ($n=3$), 95.8% ± 4.1% in Group B ($n=25$), 77.6% ± 6.3% in Group C ($n=46$) and 82.4% ± 9.2% in Group D ($n=17$) (Figure 2). OS was in 100% in Groups A and B ($n=28$), 86.8% ± 5.0% in Group C and 82.4% ± 9.2% in Group D.

Discussion

In this article, we reported the outcome of 91 childhood B-NHL and B-ALL patients treated with TCCSG NHL B9604 protocol. OS and EFS at 6 years in total were 90.1% ± 3.1% and 81.9% ± 4.4%, respectively. OS of our study was comparable with SFOP study [8], BFM study [6] and UKCCSG study [7] and better than CCG study [9] or Venezuela study [11] whereas the observation period of our study was longer than other studies. Although the EFS of our study was worse than the SFOP study [8] and BFM study [6], it was comparable with the UKCCSG study [7] and better than the CCG study [9], POG study [4] and Venezuela study [11]. Especially in patients with the most advanced disease (Group D: high BM blast cell burden and/or CNS involvement), EFS was 82.4% ± 9.2%. This was comparable with the SFOP study [8] and BFM study [6]. The overall good prognosis of this study is thought to be mainly due to the relatively larger dose of chemotherapeutic drugs and intensified regimens resulting in a good outcome.

There were 15 event cases in this study, as shown in Table III. Among these cases, the diagnosis of two relapsed patients (UPN 132,146), whose diagnosis was DLBCL by the regional hospital, was corrected to B-LBL by retrospective central review. These

Table I. Therapeutic regimen of TCCSG NHL B9604 protocol.

Group A

Block A1:

PDN 60 mg/m^2 P.O.	Days 1–5
MTX 3 g /m^2 6 h div with CFR	Days 1
CY 250 mg/m^2 1 h div	Days 2–5
VP16 100 mg/m^2 2 h div	Days 2–5
MH i.t.	Days 1

Block A2:

PDN 60 mg/m^2 P.O.	Day 1–5
VCR 1.5 mg/m^2	Day 1
AraC150 mg/m^2 × 6 1 h div q12 h	Day 1–3
CY 1 g/m^2 2 h div	Day 2,3
MH i.t.	Day 1

Group B

Block P(Prephase):

PDN 60 mg/m^2 P.O.	Day 1–5
CY 200 mg/m^2 1 h div	Day 1, 2
MH i.t.	Day 1

Block B1:

PDN 60 mg/m^2 P.O.	Day 1–5
MTX 3 g/m^2 6 h div with CFR	Day 1
CY 250 mg/m^2 1 h div	Day 2–5
VP16 100 mg/m^2 2 h div	Day 2–5
Epi 50 mg/m^2 1 h div	Day 5
MH i.t.	Day 1

Block B2:

PDN 60 mg/m^2 P.O.	Day 1–5
VCR 1.5 mg/m^2	Day 1
AraC 150 mg/m^2 × 6 1 h div q12 h	Day 1–3
CY 1 g/m^2 2 h div	Day 2,3
Epi 50 mg/m^2 1 h div	Day 5
MH i.t.	Day 1

Group C

Block P:

PDN 60 mg/m^2 P.O.	Day 1–7
VP16 100 mg/m^2 1 h div	Day 5–7
MHC i.t.	Day 1,6

Block C1:

Dex 10 mg/m^2 P.O.	Day 1–5
MTX 3 g/m^2 24 h div with CFR	Day 1
CY 250 mg/m^2 × 6 1 h div q12 h	Day 2–4
VP16 100 mg/m^2 2 h div	Day 2–5
(only day 2,3 in the first course)	
Epi 60 mg/m^2 1 h div	Day 5
MHC i.t.	Day 5 (in the first course)
MH i.t.	Day 1(in the second course)

Block C2:

Dex 10 mg/m^2 P.O.	Days 1–5
VCR 1.5 mg/m^2	Days 1
AraC 150 mg/m^2 × 6 1 h div q12 h	Days 1–3
CY 1 g/m^2 2 h div	Days 2–4
Epi 60 mg/m^2 1 h div	Days 5
MHC i.t.	Day 1
MH i.t.	Day 8 (only in the first course)

Block C3:

Dex 10 mg/m^2 P.O.	Day 1–5
VDS 3 mg/m^2	Day 1
VP16 100 mg/m^2 2 h div	Day 2–5
AraC 2 g/m^2 3 h div q12 h	Day 1–3
Epi 60 mg/m^2 1 h div	Day 5
MH i.t.	Day 1
MH i.t.	Day 8 (only in the first course)

Group D:

Block P: the same as in Group C

Block D1:

Dex 10 mg/m^2 P.O.	Day 1–5
MTX 3 g/m^2 24 h div with CFR	Day 1
CY 300 mg/m^2 × 6 1 h div q12 h	Day 2–4
(only day 2,3 in the first course)	
Epi 80 mg/m^2 1 h div	Day 5
MHC i.t.	Day 5 (in the first course)
MH i.t.	Day 1 (in the second course)
MHC i.t.	Day 8 (in the second course)
MH i.t.	Day 1,8 (in the third course)

Block D2:

Dex 10 mg/m^2 P.O.	Day 1–5
VCR 1.5 mg/m^2	Day 1
AraC 150 mg/m^2 × 6 1 h div q12 h	Day 1–3
CY 1 g/m^2 2 h div	Day 2–4
Epi 80 mg/m^2 1 h div	Day 5
MHC i.t.	Day 1 (in the first course)
MH i.t.	Day 8 (in the first course)
MH i.t.	Day 1,8 (in the second course)

Block D3:

Dex 10 mg/m^2 P.O.	Day 1–5
VDS 3 mg/m^2	Day 1
VP16 100 mg/m^2 2 h div	Day 2–5
AraC 2 g/m^2 3 h div q12 h	Day 1–3
Epi 80 mg/m^2 1 h div	Day 5
MH i.t.	Day 1,8

Cranial irradiation for patients with CNS involvement at onset
24 Gy for older than 2 years old
18 Gy for 1 year old
0 Gy for less than 1 year old

Cumulative drug dosage in each group

Group	A	B	C	D
CY (g/m^2)	4	9.4	9	11.4
VP16 (mg/m^2)	800	1200	1700	2100
MTX (g/m^2)	6	9	6	9
CA (g/m^2)	0.9	2.7	25.8	28.8
Epi (mg/m^2)	0	300	360	560

PDN, prednisolone; CFR, citrovorum factor rescue; VP16, etoposide; MH, MTX and hydrocortisone; VCR, vincristine; AraC, cytarabine; q12h, every 12 h; Epi, epirubicine; MHC, MH and AraC; Dex, dexamethazone; VDS, vindesine.

Table II. Clinical characteristics of 91 patients treated with TCCSG NHL B9604 protocol.

Registration period	April 1996–January 2001
Observation period	0–103 months (median 60 months)
Sex (Male/Female)	64/27
Age range	0.9–16.8 years (median 9.4 years)
Pathological diagnosis	Burkitt, 45
	Large cell, 26
	B-ALL, 9
	B-NHL not further specified, 6
	Others, 5
Primary site	Head and neck: 32; chest: 3
	Abdomen: 36; bone: 8
	B-ALL: 9; others: 3
Disease stage	I: 5; II: 23; III: 25; VI: 38
Risk group	A: 3; B: 25; C: 46; D:17

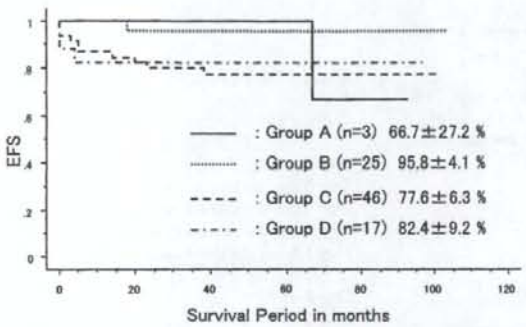

Figure 2. EFS according to the risk groups. EFS was 66.7% ± 27.2% in Group A ($n=3$), 95.8% ± 4.1% in Group B ($n=25$), 77.6% ± 6.3% in Group C ($n=46$) and 82.4% ± 9.2% in Group D ($n=17$).

patients were rescued with further chemotherapy for B-LBL. These relapses were considered due to inadequate treatment duration rather than drug resistance. In Group A, one patient (UPN 100) whose primary site was the tonsils developed diffuse large B-cell lymphoma at the cecum 5 years after initial diagnosis. Although we could not determine whether this lesion was relapse or secondary neoplasm, the EFS of Group A patients became low because of this rare event. Such a late relapse as in this case was also reported in the SFOP study [8]. Aside from these three cases, the 12 event cases consisted of three induction failures, five relapses, two toxic deaths and two second malignant neoplasm. All three induction failures and four BM involved relapsed patients died of disease progression in spite of further chemotherapy or stem cell transplantation. These cases may have required a quite different treatment concept for the first-line therapy based on stratification with tumor biology profiling. One patient (UPN 44) showed massive ICH at initial presentation and died 2 days after

Table III. Event cases in TCCSG NHL B9604 protocol.

UPN	Age	Sex	Stage	Group	Histology (central review)	Event	Remission period	Outcome	Cause of death	Survival period
11	15	F	III	C	DLBCL (DLBCL)	Secondary malignancy	14	Alive	N.A.	88+
22	5	F	III	C	Burkitt (Burkitt)	Induction failure	0	Dead	Disease progression	9
39	14	M	III	C	Burkitt (Burkitt)	Relapse (BM)	3	Dead	Disease progression	6
44	9	M	IV	D	ALL	ICH	0	Dead	ICH	0
57	11	M	IV	D	Burkitt (Burkitt)	Relapse (BM)	4	Dead	Disease progression	6
58	3	F	IV	C	Burkitt (Burkitt)	Induction failure	0	Dead	Disease progression	6
74	15	M	III	C	Burkitt (Burkitt)	Relapse (BM + local)	6	Dead	Disease progression	7
100	13	F	I	A	DLBCL (DLBCL)	Relapse (cecum)	67	Alive	N.A.	71+
102	10	F	IV	C	ALL	Relapse (BM)	6	Dead	Disease progression	11
103	2	M	III	C	Burkitt (Burkitt)	Sepsis	0	Dead	Sepsis	0
132	7	M	II	B	DLBCL (B-LBL)	Relapse (BM)	33	Alive	N.A.	66+
141	14	M	III	C	Medium (N.D.)	Relapse (local)	20	Alive	N.A.	77+
146	7	F	IV	C	DLBCL (B-LBL)	Relapse (local)	23	Alive	N.A.	60+
149	15	M	III	C	MLBCL (MLBCL)	Secondary malignancy	38	Alive	N.A.	62+
154	8	M	IV	D	Burkitt (Burkitt)	Induction failure	0	Dead	Disease progression	10

DLBCL, diffuse large B cell lymphoma; MLBCL, mediastinal large B-cell lymphoma; ICH, intracranial hemorrhage; N.A., not applicable; N.D., not done.
Age is shown in years. Remission period and survival period are shown in months. A plus sign indicates that the patient is still alive.

admission. We do not think this was therapy-related toxic death. Toxic death was reported in another patient (UPN 103) who died of sepsis during remission induction therapy. Although Grade 4 non-hematological toxicity was noted in four cases in addition to this patient, this intensified treatment regimen was well tolerated. Two second malignant neoplasm (myelodysplastic syndrome and acute myeloid leukemia) were observed 14 and 38 months after diagnosis. These patients survived with BM transplantation from unrelated donors. As we used a relatively larger dose of chemotherapeutic drugs in this study, we have to cautiously observe the development of a second malignant neoplasm among patients treated with this protocol.

In recent childhood lymphoma studies, international collaborations are essential because large scale studies are needed to prove improved outcome compared with current good one. To participate in these international studies, it is important for us (Japanese or Asian people) to confirm short, intensive chemotherapy for B-NHL and B-ALL is safe and effective regardless of racial differences. We elucidated such short, intensive chemotherapy for B-NHL and B-ALL was safe and effective for Japanese children. Treatment reduction is a main theme of childhood B-NHL therapy. Recently, Patte et al. [13] reported results of FAB/LMB96 trial for intermediate risk B-NHL patients. In this report, they elucidated a four-course treatment is enough for these patients with initial good response. Several studies for B-NHL have attempted therapy reduction to decrease toxicity, however, the dose reduction is associated with an inferior outcome for advanced stage disease so far [14,15].

The TCCSG NHL B9604 protocol achieved an excellent treatment outcome, especially in patients with the most advanced disease (Group D: high BM blast cell burden and/or CNS involvement). Although we have to cautiously observe the development of late adverse effects in treated patients, several study attempts have not succeeded in appropriate therapy reduction without jeopardizing survival and intensified regimen is, at least tentatively, needed for a good prognosis for advanced stage patients.

Acknowledgements

The authors dedicate this article to Dr. Yasunori Toyoda, who died too early, for his dedication to their lymphoma studies. This study was done on behalf of the Tokyo Children's Cancer Study Group (TCCSG). The authors thank Mrs. Kaori Itagaki for preparing and refining the protocol data for non-Hodgkin lymphoma in the Tokyo Children's Cancer Study Group.

References

1. Jaffe ES, Harris NL, Stein H, Vardiman JW. WHO Classification of Tumours of Haematopoietic and Lymphoid Tissues. Lyon, France: International Agency for Research on Cancer (IARC); 2001.
2. Gasparini M, Lombardi F, Gianni MC, Lattuada A, Rilke F, Fossati-Bellani F. Childhood non-Hodgkin's lymphoma: prognostic relevance of clinical stage and histologic subgroups. Am J Pediatr Hematol Oncol 1983;5:161–171.
3. Anderson J, Jenkin RD, Wilson JF, Kjerdberg CR, Sposto R, Chilcote RR, et al. Long-term follow up of patients treated with COMP or LSA2L2 therapy for childhood non-Hodgkin's lymphoma: a report of CCG-551 from the Children's Cancer Group. J Clin Oncol 1993;11:1024–1032.
4. Bowman WP, Shuster JJ, Cook B, Griffin T, Behm F, Pullen J, et al. Improved survival for children with B-cell acute lymphoblastic leukemia and stage IV small noncleaved-cell lymphoma: a Pediatric Oncology Group study. J Clin Oncol 1996;14:1252–1261.
5. Brecher ML, Schwenn MR, Coppes MJ, Bowmann WP, Link MP, Berard CW, et al. Fractionated cyclophosphamide and back to back high dose methotrexate and cytosine arabinoside improves outcome in patients with stage III high grade small non-cleaved cell lymphomas (SNCCL): a randomized trial of the Pediatric Oncology Group. Med Pediatr Oncol 1997;29:526–533.
6. Reiter A, Schrappe M, Tiemann M, Ludwig WD, Yakisan E, Zimmermann M, et al. Improved treatment results in childhood B-cell neoplasms with tailored intensification of therapy: a report of Berlin–Frankfurt–Munster Group Trial BFM 90. Blood 1999;49:3294–3306.
7. Atra A, Imeson JD, Hobson R, Gerrard M, Hann IM, Eden OB, et al. Improved outcome in children with advanced stage B-cell non-Hodgkin's lymphoma (B-NHL): results of the United Kingdom Children Cancer Study Group (UKCCSG) B9002 protocol. Br J Cancer 2000;82:1396–1402.
8. Patte C, Auperin A, Michon J, Behrendt H, Leverger G, Freppaz D, et al. The Societe Francasie d'Oncologie Pediatrique LMB89 protocol: highly effective multiagent chemotherapy tailored the tumor burden and initial response in 561 unselected children with B-cell lymphomas and L3 leukemia. Blood 2001;97:3370–3379.
9. Cairo MS, Krailo MD, Morse M, Hutchinson RJ, Harris RE, Kjerdsberg CR, et al. Long-term follow-up of short intensive multiagent without high-dose methotrexate ('Orange') in children with advanced non-lymphoblastic non-Hodgkin's lymphoma: a Children's Cancer Group report. Leukemia 2002;16:594–600.
10. Spreafico F, Massimino M, Luksch R, Riccardi R, Tesoro-Tess JD, Gandola L, et al. Intensive very short chemotherapy for advanced Burkitt's lymphoma in children. J Clin Oncol 2002;20:2783–2788.
11. Acquatella G, Insausti CL, Garcia R, Gomez R, Hernandez M, Carneiro M, et al. Outcome of children with B cell lymphoma in Venezuela with the LMB-89 protocol. Pediatr Blood Cancer 2004;43:580–586.
12. Murphy SB. Classification, staging and end results of treatment in childhood non-Hodgkin's lymphoma: dissimilarities from lymphomas in adults. Semin Oncol 1980; 7:332–339.
13. Patte C, Auperin A, Gerrard M, Michon J, Pinkerton R, Sposto R, et al. Results of the randomized international trial of LMB-96 trial for intermediate risk B-cell non-Hodgkin lymphoma in children and adolescents: it is possible to reduce treatment for the early responding patients. Blood 2007; 109:2773–2780.

14. Woessmann W, Seidemann K, Mann G, Zimmermann M, Burkhardt B, Oschlies I, et al. The impact of the methotrexate administration schedule and dose in the treatment of children and adolescents with B-cell neoplasms: a report from the BFM group study NHL-BFM95. Blood 2005;105:948–958.

15. Cairo MS, Gerrard M, Sposto R, Auperin A, Pinkerton R, Michon J, et al. Results of a randomized international study of high-risk central nervous system B non-Hodgkin lymphoma and B acute lymphoblastic leukemia in children and adolescents. Blood 2007;109:2736–2743.

MOLECULAR AND CELLULAR BIOLOGY, Apr. 2008, p. 2125–2137 Vol. 28, No. 7
0270-7306/08/$08.00+0 doi:10.1128/MCB.00740-07

Inducible Expression of Chimeric EWS/ETS Proteins Confers Ewing's Family Tumor-Like Phenotypes to Human Mesenchymal Progenitor Cells▽†

Yoshitaka Miyagawa,[1] Hajime Okita,[1]* Hideki Nakaijima,[1] Yasuomi Horiuchi,[1] Ban Sato,[1] Tomoko Taguchi,[1] Masashi Toyoda,[3] Yohko U. Katagiri,[1] Junichiro Fujimoto,[2] Jun-ichi Hata,[1] Akihiro Umezawa,[3] and Nobutaka Kiyokawa[1]

Department of Developmental Biology, National Research Institute for Child Health and Development, 2-10-1, Okura, Setagaya-ku, Tokyo 157-8535, Japan[1]; National Research Institute for Child Health and Development, 2-10-1, Okura, Setagaya-ku, Tokyo 157-8535, Japan[2]; and Department of Reproductive Biology, National Research Institute for Child Health and Development, 2-10-1, Okura, Setagaya-ku, Tokyo 157-8535, Japan[3]

Received 27 April 2007/Returned for modification 13 July 2007/Accepted 7 January 2008

Ewing's family tumor (EFT) is a rare pediatric tumor of unclear origin that occurs in bone and soft tissue. Specific chromosomal translocations found in EFT cause EWS to fuse to a subset of ets transcription factor genes (ETS), generating chimeric EWS/ETS proteins. These proteins are believed to play a crucial role in the onset and progression of EFT. However, the mechanisms responsible for the EWS/ETS-mediated onset remain unclear. Here we report the establishment of a tetracycline-controlled EWS/ETS-inducible system in human bone marrow-derived mesenchymal progenitor cells (MPCs). Ectopic expression of both EWS/FLI1 and EWS/ERG proteins resulted in a dramatic change of morphology, i.e., from a mesenchymal spindle shape to a small round-to-polygonal cell, one of the characteristics of EFT. EWS/ETS also induced immunophenotypic changes in MPCs, including the disappearance of the mesenchyme-positive markers CD10 and CD13 and the up-regulation of the EFT-positive markers CD54, CD99, CD117, and CD271. Furthermore, a prominent shift from the gene expression profile of MPCs to that of EFT was observed in the presence of EWS/ETS. Together with the observation that EWS/ETS enhances the ability of cells to invade Matrigel, these results suggest that EWS/ETS proteins contribute to alterations of cellular features and confer an EFT-like phenotype to human MPCs.

Ewing's family tumor (EFT) is a rare childhood cancer arising mainly in bone and soft tissue. Since EFT has a poor prognosis, it is important to elucidate the underlying pathogenic mechanisms for establishing a more effective therapeutic strategy. EFT is characterized by the presence of chimeric genes composed of EWS and ets transcription factor genes (ETS) formed by specific chromosomal translocations, i.e., EWS/FLI1, t(11;22)(q24;q12); EWS/ERG, t(21;22)(q12;q12); EWS/ETV1, t(7;22)(p22;q12); EWS/E1AF, t(17;22)(q12;q12); and EWS/FEV, t(2;22)(q33;q12) (26). The products of these chimeric genes behave as aberrant transcriptional regulators and are believed to play a crucial role in the onset and progression of EFT (3, 36). Indeed, recent studies have revealed that the induction of EWS/FLI1 proteins can trigger transformation in certain cell types, including NIH 3T3 cells (36), C2C12 myoblasts (12), and murine primary bone marrow-derived mesenchymal progenitor cells (MPCs) (6, 45, 52). However, studies have also indicated that overexpression of EWS/FLI1 provokes apoptosis and growth arrest in mouse normal embryonic fibroblasts and primary human fibroblasts (10, 31), hence hampering understanding of the precise role of EWS/ETS proteins in the development of EFT. The function of EWS/ETS proteins would be greatly influenced by cell type, and thus the cells that can originate EFTs might be more susceptible to the tumorigenic effects of EWS/ETS.

Although the cell origin of EFT is still unknown, the expression of neuronal markers in spite of the occurrence in bone and soft tissues has kept open the debate as to a potential mesenchymal or neuroectodermal origin. As described above, ectopic expression of EWS/FLI1 results in dramatic changes in morphology and the formation of EFT-like tumors in murine primary bone marrow-derived MPCs but not in murine embryonic stem cells (6, 45, 52), supporting the notion that MPCs are a plausible cell origin of EFT (45). However, others argue that MPCs cannot be considered progenitors of EFT without further evidence of similarity between human EFT and MPC-EWS/FLI1-induced tumors in mice (29, 46).

The development of experimental systems using murine species is useful for elucidating the mechanisms behind the pathogenesis of EFT. However, several differences between human and murine systems cannot be ignored; these differences include the expression patterns of surface antigens in MPCs, for instance (7, 44, 51, 53). Moreover, human cells are difficult to transform in vitro, and the transformed cells of mice seem to produce a more aggressive tumor than those of hu-

* Corresponding author. Mailing address: Department of Developmental Biology, National Research Institute for Child Health and Development, 2-10-1, Okura, Setagaya-ku, Tokyo 157-8535, Japan. Phone: 81-3-3416-0181. Fax: 81-3-3417-2496. E-mail: okita@nch.go.jp.

† Supplemental material for this article may be found at http://mcb.asm.org/.

▽ Published ahead of print on 22 January 2008.

TABLE 1. Cell lines used in this study and fusion transcript types

Cell line	Diagnosis	Fusion transcript type	Reference
EES-1	EFT	EWS/FLI1 type I	20
SCCH196	EFT	EWS/FLI1 type I	21
RD-ES	EFT	EWS/FLI1 type II	5
SK-ES1	EFT	EWS/FLI1 type II	5
NCR-EW2	EFT	EWS/FLI1 type II	19
NCR-EW3	EFT	EWS/E1AF	19
W-ES	EFT	EWS/ERG	13
NB69	NB		15
NB9	NB		15
GOTO	NB		47
NRS-1	RMS	PAX3/FKHR	40

mans (1). The findings suggest the existence of undefined cell-autonomous mechanisms that render human cells resistant to malignant transformation. Therefore, the use of human cell models is ideal for clarifying how EFT develops. Models of the onset of EFT have been generated using primary fibroblasts (31) and rhabdomyosarcoma cells (23). However, these cell types are not appropriate for studying the origins of EFT, and a model that precisely recapitulates EWS/ETS-mediated EFT formation is required.

UET-13 cells are obtained by prolonging the life span of human bone marrow stromal cells by use of the retroviral transgenes hTERT and E7 (38, 50), retain the ability to differentiate into not only mesodermal derivatives but also neuronal progenitor-like cells, and are considered a good model for studying the cellular events in human MPCs. Therefore, we have examined the biological effect of EWS/ETS in human MPCs by use of UET-13 cells by exploiting tetracycline-inducible systems for expressing EWS/ETS (EWS/FLI1 and EWS/ERG). Here we report that overexpression of EWS/ETS mediates an EFT-like phenotype, including morphology, immunophenotype, and gene expression profile, with enhancement of the Matrigel invasion ability of UET-13 cells.

MATERIALS AND METHODS

Cell cultures and establishment of UET-13TR-EWS/ETS cell lines. UET-13 cells were cultured in Dulbecco's modified Eagle's medium (DMEM) with 10% Tet system approved fetal bovine serum (T-FBS) (Takara) at 37°C under a humidified 5% CO_2 atmosphere. EFT cell lines (EES-1 [20], SCCH196 [21], RD-ES and SK-ES1 [5], NCR-EW2 and NCR-EW3 [19], and W-ES [13]) and neuroblastoma (NB) cell lines (NB69 and NB9 [15] and GOTO [47]) were cultured in RPMI 1640 with 10% FBS. A rhabdomyosarcoma cell line, NRS-1 (40), was cultured in Eagle's minimal essential medium with 10% FBS. The cell lines used in this study are listed in Table 1.

UET-13 cells were seeded at a density of 5×10^4 cells per well in 24-well tissue culture plates 1 day prior to transfection. For introducing the tetracycline-inducible system, UET-13 cells were transfected with pcDNA6-TR (Invitrogen) by use of Lipofectamine 2000 (Invitrogen). After 72 h, the medium was replaced with fresh medium containing 200 μg/ml of blasticidin S (Invitrogen). Individual resistant clones were selected for a month and designated UET-13TR cells. UET-13TR cells were further transfected with pcDNA4-EWS/ETSs constructed as described below, and individual resistant clones were selected in DMEM containing 10% T-FBS and 200 to 300 μg/ml of Zeocin (Invitrogen). The Zeocin-resistant clones were expanded and tested for the induction of EWS/ETS expression upon the addition of tetracycline by use of reverse transcription-PCR (RT-PCR) as described below.

Plasmid construction. A gateway cassette (bases 1 to 1705) was amplified from pBLOCK-IT3-DEST (Invitrogen) by PCR, and the PCR product was inserted into the EcoRV site of pcDNA4-TO (Invitrogen) (termed pcDNA4-DEST). Since the type II EWS/FLI1 is a stronger transactivator than the type I product (32), we used the type II variant in the present study. EWS/ERG was isolated from W-ES, an EFT cell line, joining EWS exon 7 and ERG exon 9. Full-length EWS/FLI1 type II and EWS/ERG cDNAs were amplified from cDNAs prepared from NCR-EW2 and W-ES cells, respectively, by PCR as described below and cloned into the XmnI-EcoRV sites of pENTR11 (Invitrogen). The resulting pENTR11-EWS/ETSs were recombined with pcDNA4-DEST by use of LR recombination reaction as instructed by the manufacturer (Invitrogen) to construct the tetracycline-inducible EWS/ETS expression vector pcDNA4-EWS/ETSs.

Western blot analysis. UET-13 transfectants were cultivated with or without 3 μg/ml of tetracycline for 72 h. Western blot analysis was performed as previously described (37). Briefly, the cell lysates were prepared and separated on a 10% sodium dodecyl sulfate-polyacrylamide gel electrophoresis gel and transferred onto a polyvinylidene difluoride membrane. The membranes were blocked with 5% skimmed milk in phosphate-buffered saline (PBS) containing 0.01% Tween 20 (Sigma) and incubated with primary antibodies. As the primary antibodies, anti-Fli-1, anti-Erg-1/2/3 (Santa Cruz Biotechnology), and anti-actin (Sigma) were used. Horseradish peroxidase-conjugated anti-rabbit or anti-mouse immunoglobulin G (IgG) antibodies (DakoCytomation) were used as secondary antibodies. Blots were detected by chemiluminescence using an ECL Plus Western blotting detection system (GE Healthcare Bio-Science Corp.) and exposed to X-ray film (Kodak) for 5 to 30 min.

MTT assay and detection of apoptosis. Growth curves of UET-13 transfectants were determined using the 3-(4,5-dimethylthiazol-2-yl)-2,5-diphenyltetrazolium bromide (MTT) assay as described previously (18). The apoptosis was detected using an annexin V-fluorescein isothiocyanate (FITC) apoptosis detection kit (Biovision) according to the manufacturer's instructions and analyzed by flow cytometry (Cytomics FC500; Beckman Coulter).

Immunofluorescence analysis. After 1 week of culture in the absence or presence of tetracycline, UET-13 cells and the transfectants were harvested with 0.25% trypsin plus EDTA (IBL). The cells (2×10^5) were incubated with mouse monoclonal antibodies for 20 min. In the case of fluorescence-labeled antibodies, the cells were washed with PBS and then analyzed. In the case of primary unconjugated mouse antibodies, the cells were washed and then incubated with FITC-conjugated goat anti-mouse IgG antibody (Jackson ImmunoResearch Laboratories) for 20 min. Cell fluorescence was detected using a Cytomics FC500 instrument as described previously (27).

Antibodies against the following human antigens were used: CD10, CD13, CD14, CD29, CD34, CD40, CD44, CD45, CD49e, CD54, CD56, CD61, CD90, CD105, CD117, and CD166 from Beckman Coulter; CD73 from BD Biosciences-Pharmingen; CD55 from Abcam; CD59 from Cedarlane Laboratories; and CD133 and CD271 from Miltenyi Biotec GmbH.

Immunocytochemistry. Cells were grown on collagen type I-coated cover glasses (Iwaki). After 72 h with or without tetracycline, cells were fixed for 30 min in 4% paraformaldehyde and permeabilized in PBS containing 0.2% Triton X-100 (Sigma) for 30 min. Subsequently, they were washed with PBS and blocked in PBS containing 0.1% Triton X-100 and 1% bovine serum albumin (Sigma) for 30 min before being incubated with a monoclonal anti-CD99 antibody, i.e., 12E7 (1:100) (DakoCytomation) or O13 (1:200) (Thermo), and polyclonal anti-Fli-1 antibody (1:100) (Santa Cruz) for 1 h. Bound antibodies were visualized with appropriate secondary antibodies, i.e., Alexa Fluor 488 goat anti-mouse IgG (heavy plus light chains) highly cross-adsorbed and Alexa Fluor 546 goat anti-rabbit IgG (heavy plus light chains) highly cross-adsorbed (Invitrogen) for 1 h at 1:300. Nuclei were counterstained with 4′,6′-diamidino-2-phenylindole (DAPI) or propidium iodide (PI) (Sigma). For the visualization of whole cells, cells were treated with Celltracker Blue (Invitrogen) for 30 min and then fixed. Fluorescence was observed and analyzed using a confocal laser scanning microscope and image software (either FV500 from Olympus or LSM510 from Carl Zeiss). Precise measurements of cell size, nuclear size, and the nucleus-to-cytoplasm (N/C) ratio were performed using Image J (16).

RT-PCR analysis. Total RNA was extracted from cells by use of an RNeasy kit (Qiagen) and reverse transcribed using a first-strand cDNA synthesis kit (GE Healthcare Bio-Science Corp). RT-PCR was performed with a HotstarTaq master mix kit (Qiagen). As an internal control, human GAPDH cDNA was also amplified. The sequences of gene-specific primers for RT-PCR were as follows: for EWS/FLI1 (forward), 5′-ATGGCGTCCACGGATTACAGTACCT-3′; for EWS/FLI1 (reverse), 5′-GGGTCTTCTTTGACACTCAATCG-3′; for EWS/ERG (forward), 5′-ATGGCGTCCACGGATTACAGTACCT-3′; for EWS/ERG (reverse), 5′-TTAGTAGTAAGTGCCCAGATGAGAA-3′; for GAPDH (forward), 5′-CCACCCATGGCAAATTCCATGGCA-3′; and for GAPDH (reverse), 5′-TCTAGACGGCAGGTCAGGT/CCACC-3′. PCR products were electrophoresed with a 1% agarose gel and stained with ethidium bromide.

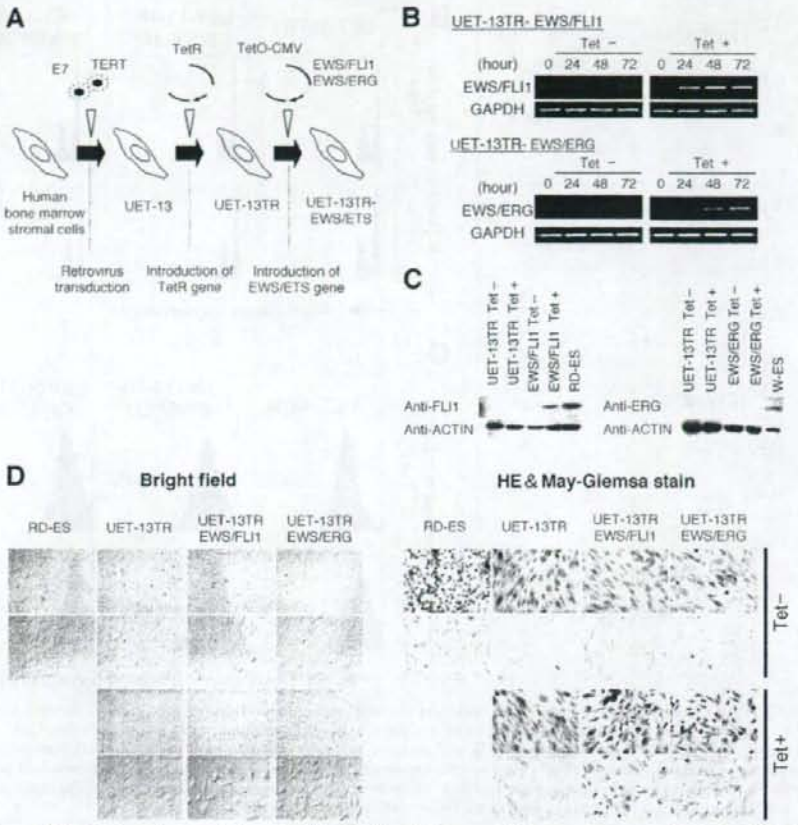

FIG. 1. The effect of EWS/ETS on the morphology of UET-13 cells. (A) The establishment of a tetracycline-inducible EWS/ETS expression system in UET-13 cells. CMV, cytomegalovirus. (B) Analyses for confirming the inducible expression of EWS/ETS genes. EWS/ETS mRNAs were detected in UET-13 transfectants UET-13TR-EWS/FLI1 and UET-13TR-EWS/ERG by RT-PCR. These cells were treated with or without 3 μg/ml of tetracycline (Tet) for the indicated periods. As an internal control, a human GAPDH gene was used. (C) Analyses for confirming the inducible expression of EWS/ETS proteins. The cells were treated as described for panel B and subjected to Western blotting for the detection of EWS/ETS proteins. The extracts of RD-ES and W-ES cells were also examined as positive controls. Membranes were reprobed with anti-actin antibody as a loading control. (D) Morphological change after tetracycline treatment of UET-13 transfectants. UET-13 cells and the transfectants were cultured in the absence or presence of tetracycline for 72 h and observed by light microscopy. Magnification, ×40 (top); ×200 (bottom). Cells were also examined using hematoxylin-eosin (HE) (top) and May-Giemsa (bottom) staining (magnification, ×200).

Real-time RT-PCR. Real-time RT-PCR was performed using TaqMan universal PCR master mix and TaqMan gene expression assays and an inventoried assay on an ABI Prism 7900HT sequence detection system (Applied Biosystems) according to the manufacturer's instructions. The human GAPDH gene was used as an internal control for normalization.

DNA microarray analysis. Total RNA isolated from cells was reverse transcribed and labeled using one-cycle target labeling and control reagents as instructed by the manufacturer (Affymetrix). The labeled probes were hybridized to the human genome U133 Plus 2.0 array (Affymetrix). The arrays were performed in a single experiment and analyzed using GeneChip operating software, version 1.2 (Affymetrix). Background subtraction, normalization, and principal component analysis (PCA) were performed by GeneSpring GX 7.3 software (Agilent Technologies). Signal intensities were prenormalized based on the median of all measurements on that chip. To account for the difference in detection efficiencies between the spots, prenormalized signal intensities on each gene were normalized to the median of prenormalized measurements for that gene. The data were filtered using the following steps. (i) Genes that were scored as absent in all samples were eliminated. (ii) Genes for which the signal intensities were lower than 100 were eliminated. (iii) Performing cluster analysis using filtering genes, we selected the genes that exhibited increased expression or decreased expression in tetracycline-treated cells. Accession numbers for the microarray data are given below.

Invasion assay. The invasion assay was performed using Matrigel (BD Bioscience) according to the previous description (34) with some modification. Polycarbonate filter inserts containing 8-μm pores (BD Falcon) were coated with 50 μl of a 6:1 mixture of culture medium and Matrigel and placed into 24-well culture plates containing DMEM supplemented with 10% T-FBS as chemoattractants. Cells (2.5×10^4) treated with or without tetracycline for 72 h were suspended in DMEM containing 0.01% T-FBS and plated on top of each filter insert. After 20 h in culture in the presence or absence of tetracycline, noninvading cells were removed from upper surface of the filter with a cotton swab. The invading cells on the lower surface of the filter were fixed with formalin, stained with hematoxylin-eosin, and counted in five fields per membrane with light microscopy. As a control, cells were also cultured on uncoated filter inserts. The invasion efficiency was presented as the ratio of the number of invading cells on Matrigel-coated inserts to that on uncoated inserts. Experiments were performed in triplicate, and the means with standard deviations of the values are shown in the graphs in Fig. 8.

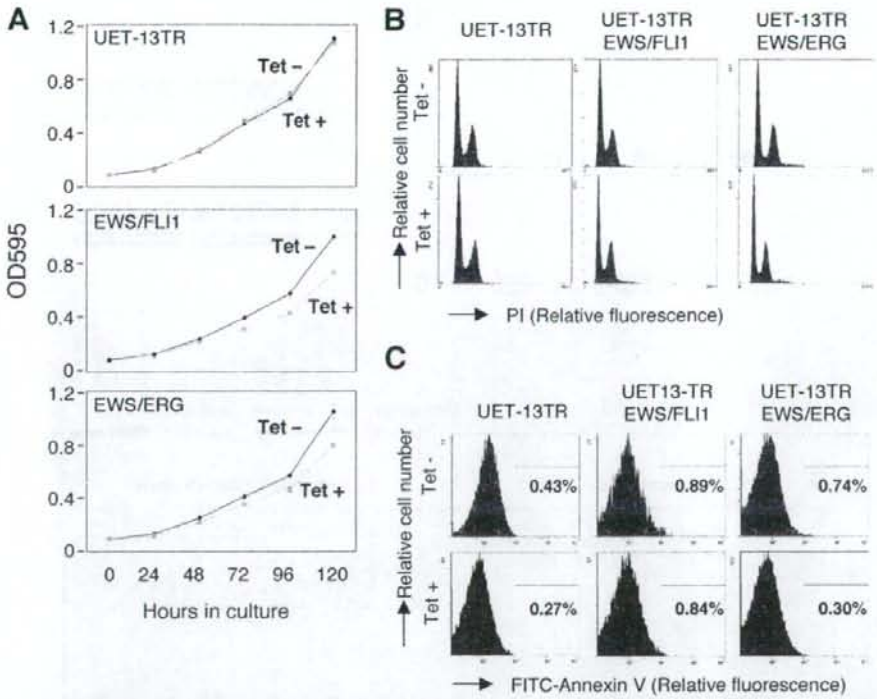

FIG. 2. Effects of EWS/ETS on cell growth in UET-13 cells. (A) Growth curve for UET-13 transfectants. Cells were seeded at 10^5/well and cultured as described for Fig. 1. The increase in cell number was analyzed by MTT assay. Values are means with the standard errors (SE) from three independent experiments. Diamond symbols indicate UET-13 transfectants in the absence of tetracycline (Tet); box symbols indicate UET-13 transfectants in the presence of tetracycline. (B) Cells were cultured as described for panel A in the absence or presence of tetracycline for 3 days and then stained with PI, and DNA contents were analyzed by flow cytometry (*x* axis, relative intensity of fluorescence; *y* axis, relative cell number). (C) Cells treated as described for panel B were stained with FITC-annexin V and analyzed.

Microarray data accession numbers. Microarray data have been deposited in the Gene Expression Omnibus database GEO (www.ncbi.nlm.nih.gov/geo) (accession numbers GSE8665 and GSE8596).

RESULTS

EWS/ETS expression results in morphological changes in UET-13 cells. To investigate how the expression of EWS/ETS affects human MPCs, we used UET-13 cells as a model of human MPCs and expressed EWS/FLI1 (UET-13TR-EWS/FLI1) and EWS/ERG (UET-13TR-EWS/ERG) in a tetracycline-inducible manner (Fig. 1A). As shown in Fig. 1B and C, we confirmed that the tetracycline treatment could induce EWS/ETS expression by RT-PCR analysis and Western blotting. The inducibility upon the addition of doxycycline was comparable to that upon the addition of tetracycline.

Using these cell systems, first we examined the effect of EWS/ETS expression on morphology in UET-13 transfectants. When tetracycline was added to the culture, the morphologies of both UET-13TR-EWS/FLI1 and UET-13TR-EWS/ERG cells were dramatically changed (Fig. 1D). Tetracycline-treated UET-13TR-EWS/ETS cells consisted of a mixture of small round-to-polygonal cells and short spindle cells. The cell morphology resembled that of EFT cell lines. To assess the reproducibility of this phenotypic change, other UET-13TR-EWS/ETS clones were examined, and similar morphological changes were observed. Since tetracycline treatment did not affect the morphology of UET-13TR cells (Fig. 1D), it was suggested that the morphological alteration in UET-13 cells from a mesenchymal cell shape to small round cells, one of the characteristics of EFT, can be attributed to EWS/ETS expression.

EWS/ETS expression inhibits cell growth in UET-13 cells. Next, the effect of EWS/ETS expression on the growth of UET-13 cells was analyzed. As shown in Fig. 2A, an MTT assay revealed that the addition of tetracycline had no effect on the growth of UET-13TR cells but slightly inhibited that of UET-13TR-EWS/ETS cells. We also assessed the cell growth of UET-13 transfectants after tetracycline addition by cell counting and obtained results well in accord with those from the MTT assay (data not shown). To determine the mechanism of this inhibition, DNA content and the binding of annexin V to UET-13 transfectants were examined. No significant increase in either sub-G_1-phase cells (Fig. 2B) or annexin V binding cells (Fig. 2C) was detected, suggesting that EWS/ETS-mediated growth inhibition in UET-13 cells was not due to the activation of an apoptotic pathway. Moreover, no significant decrease in S-G_2-phase cells was observed (Fig. 2B).

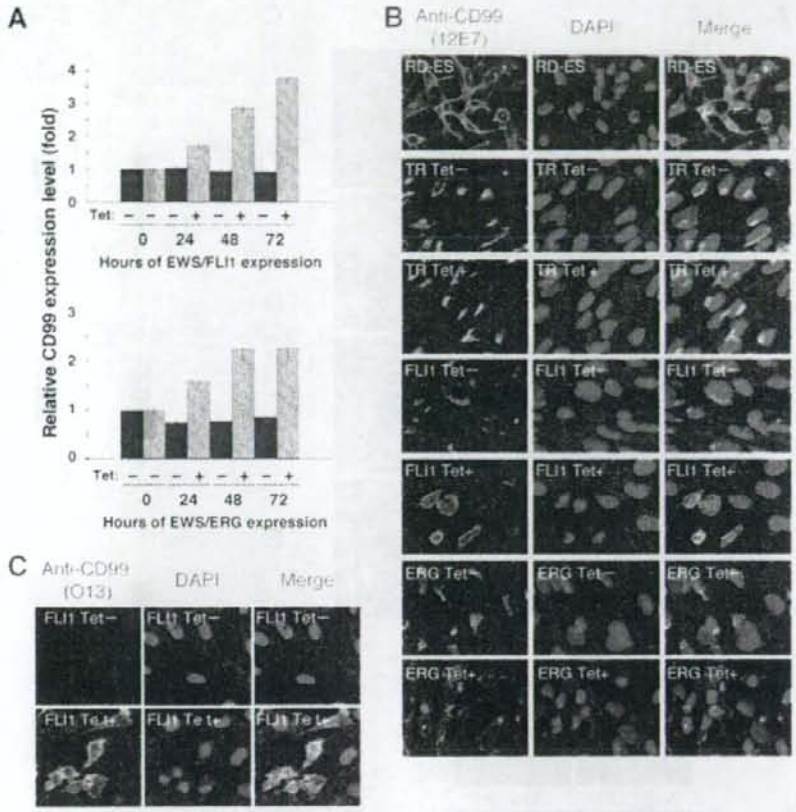

FIG. 3. Effects of tetracycline-mediated EWS/ETS expression on the expression and distribution of CD99 in UET-13 cells. (A) Relative CD99 levels in UET-13 transfectants in the absence or presence of tetracycline (Tet). UET-13 transfectants were treated with or without 3 μg/ml of tetracycline for the indicated periods. Real-time RT-PCR was performed to investigate the expression pattern of CD99. Signal intensities of CD99 were normalized using those of a control housekeeping gene (human GAPDH gene). Data are relative values with standard deviations from triplicate wells and are normalized to the mRNA level at 0 h, which is arbitrarily set to 1 in the graphical presentation. (B and C) Immunocytostaining of CD99 in UET-13 transfectants. Cells were cultured on coverslips in the absence or presence of tetracycline for 72 h and then stained with anti-CD99 antibody 12E7 (B) or O13 (C) as described in Materials and Methods. RD-ES cells were also examined as a positive control. For the staining of nuclei, DAPI was used.

Effect of EWS/ETS on CD99 expression in UET-13 cells. The p30/32MIC-2 gene product, CD99, is a cell surface glycoprotein expressed in EFT with a strong membranous staining pattern and thus constitutes a useful marker for EFT (2, 30). Knowing the dramatic change of morphology in UET-13 cells, we next investigated the mRNA level of CD99 in tetracycline-treated and untreated UET-13 transfectants by quantitative real-time RT-PCR. CD99 levels were clearly elevated by tetracycline treatment in both UET-13TR-EWS/FLI1 and UET-13TR-EWS/ERG cells in a time-dependent manner (Fig. 3A).

We also examined the protein expression of CD99 by immunostaining using 12E7 antibody, which is most widely used as an anti-CD99 antibody. An EFT cell line, RD-ES, showed strong membranous staining of CD99 (Fig. 3B), while neither UET-13TR cells nor UET-13 cells had such a staining. Of note is the fact that although 12E7 reactivity was observed only in the cytoplasm in perinuclear regions in both UET-13TR (Fig. 3B) and UET-13 (data not shown) cells, this antibody is well known to cross-react with a cytoplasmic protein not yet characterized. Since another anti-CD99 antibody, O13, did not react with either UET-13TR (Fig. 3C) or UET-13 (data not shown) cells, we concluded that the perinuclear staining of 12E7 mentioned above was a cross-reaction with unrelated proteins.

In the absence of tetracycline, both UET-13TR-EWS/FLI1 and UET-13TR-EWS/ERG cells were also negative with anti-CD99 antibodies (a pattern designated $CD99^-$), similar to UET-13 cells. Surprisingly, however, tetracycline induced a membranous staining pattern (designated $CD99^+$) in UET-13TR-EWS/FLI1 and UET-13TR-EWS/ERG cells, and some $CD99^+$ cells had irregularly contoured nuclei (Fig. 3B). The same results were observed with another anti-CD99 antibody, O13 (Fig. 3C), indicating that the membranous staining observed for UET-13 transfectants with the anti-CD99 antibodies

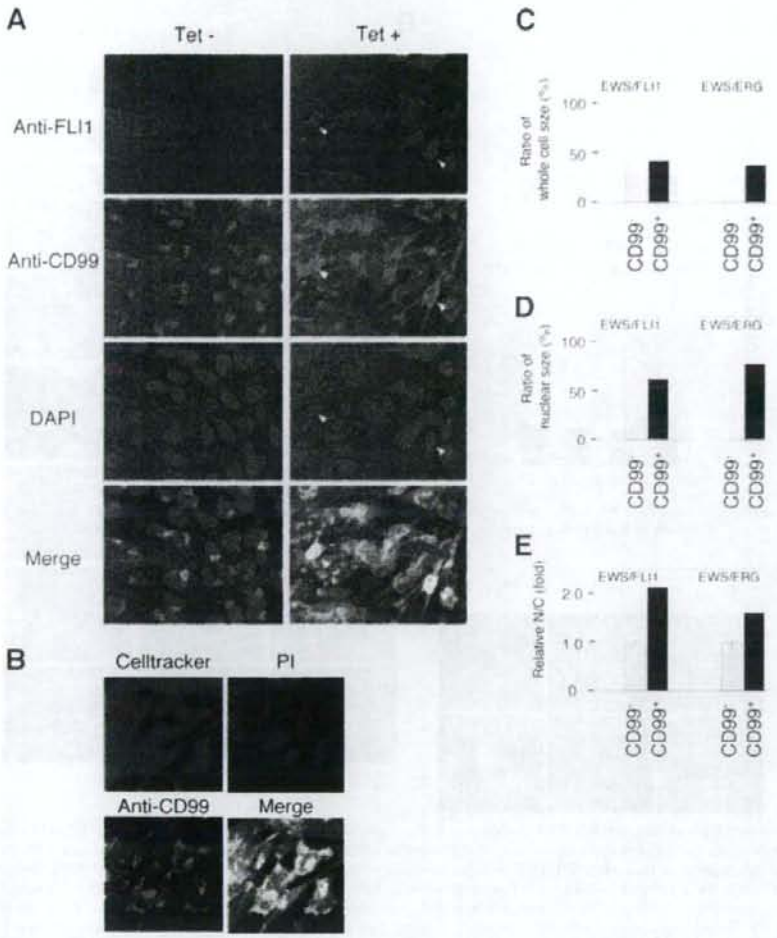

FIG. 4. EWS/ETS expression, alteration of CD99 distribution, and cell morphological changes in UET-13 cells. (A) Immunofluorescence studies using anti-Fli1 (red), anti-CD99 (green), and DAPI (blue). UET-13TR-EWS/FLI1 cells were cultured on coverslips in the absence or presence of tetracycline (Tet) for 72 h and then stained as described in Materials and Methods. White arrowheads indicate $CD99^+$ cells that have a strong staining pattern with anti-Fli1 antibodies and also have remarkable CD99 expression and morphological features. (B) Immunofluorescence analysis by triple staining with whole cells (Celltracker; blue), CD99 (anti-CD99; green), and nuclei (PI; red). UET-13TR-EWS/FLI1 cells were cultured as described for panel A and then stained as described in Materials and Methods. (C to E) Measurements of whole-cell size (C), nuclear size (D), and N/C ratio (E) in tetracycline-treated UET-13 transfectants. UET-13TR-EWS/FLI1 and UET-13TR-EWS/ERG cells were cultured on coverslips in the presence of tetracycline for 72 h and then stained as described in Materials and Methods. These samples were analyzed by the image analysis software Image J ($n = 50$). (C and D) Data are relative values with the SE and are normalized to the size of $CD99^-$ cells, which is arbitrarily set to 100. (E) Data are relative values with the SE and are normalized to the size of $CD99^-$ cells, which is arbitrarily set to 1.

was really CD99 derived. Despite the fact that cells were single colony derived, there was a heterogeneous response to tetracycline treatment in UET-13TR-EWS/FLI1 and UET-13TR-EWS/ERG cells, but most of the $CD99^+$ cells had a small round morphology, one of the characteristics of EFT. To assess the correlation between EWS/FLI1 expression and the change of the CD99 expression pattern, we performed immunofluorescence studies using anti-Fli1 and anti-CD99 antibodies. As shown in Fig. 4A, tetracycline treatment induced a marked enhancement of nuclear staining with anti-Fli1 antibodies in a large number of UET-13TR-EWS/FLI1 cells, indicating the induction of EWS/FLI1 proteins. Furthermore, we observed that the cells with a strong signal for Fli1 tended to reveal a membranous staining pattern with anti-CD99 antibodies and a small round morphology (Fig. 4A). To further verify the correlation between CD99 expression pattern and cell morphology, we estimated the size of cells by triple staining using Celltracker Blue, PI, and anti-CD99 antibody (Fig. 4B). As

TABLE 2. Immunophenotypic characterization of UET-13 transfectants and EFT cells

MPC status[a]	CD marker	Result for[b]: UET-13	UET-13TR		UET-13TR-EWS/FLI1		UET-13TR-EWS/ERG		RD-ES	EFT status[c]	SK-ES1
		Tet$^-$	Tet$^+$	Tet$^-$	Tet$^+$	Tet$^-$	Tet$^+$				
M+	CD29	+	+	+	+	+	+	+	+	+	
M+	CD59	+	+	+	+	+	+	+	+	+	
M+	CD90	+	+	+	+	+	+	+	+	+	E+
M+	CD105	+	+	+	+	+	+	+	+	+	
M+	CD166	+	+	+	+	+	+	+	+	+	
M+	CD44	+	+	+	+	+	+	+	−	−	
M+	CD73	+	+	+	+	+	+	+	−	−	
M+	**CD10**	+	+	+	+	**Down**	+	**Down**	−	−	
M+	**CD13**	+	+	+	+	**Down**	+	**Down**	−	−	
M+	**CD49e**	+	+	+	+	**Down**	+	**Down**	+	−	
M+	**CD61**	+	+	+	+	**Down**	+	**Down**	−	−	
M+	**CD55**	+	+	+	+	**Down**	+	+	+	−	
M+	**CD54**	−	−	−	−	**Up**	−	**Up**	+	+	E+
M(−)	**CD117**	−	−	−	−	**Up**	−	**Up**	+	+	E+
M+/−	**CD271**	−	−	−	−	**Up**	−	**Up**	+	+	E+
	CD40	−	−	−	−	−	−	−	+	+	E+
	CD56	−	−	−	−	−	−	−	+	+	E+
M(−)	CD133	−	−	−	−	−	−	−	+	+	
M(−)	CD14	−	−	−	−	−	−	−	−	−	
M(−)	CD34	−	−	−	−	−	−	−	−	−	
M(−)	CD45	−	−	−	−	−	−	−	−	−	

[a] M(−), negative for MPCs; M+/−, positive for BM-derived MPCs but negative after in vitro culture; M+, positive for MPCs.
[b] +, most cells positive; −, negative; Up, up-regulated by tetracycline treatment; Down, down-regulated by tetracycline treatment. Boldface indicates the antigens the immunophenotypes of which were changed in favor of EFT. Tet$^-$, tetracycline negative; Tet$^+$, tetracycline positive.
[c] E+, positive for EFTs.

presented in Fig. 4C and D, the results clearly showed that the majority of CD99$^+$ cells were significantly smaller in both whole-cell size and nuclear size than the CD99$^-$ cells. Moreover, CD99$^+$ cells also had a substantially increased N/C ratio (Fig. 4E). These results indicated that EWS/ETS expression promoted CD99 expression in UET-13 cells, and CD99 expression status is correlated with the degree of morphological change.

EWS/ETS expression altered the immunophenotype of UET-13 cells. Human MPCs reveal a characteristic expression of several surface antigens and can be identified on the basis of the reactivity with a set of monoclonal antibodies against CD antigens (25, 42). On the other hand, some CD antigens are characteristically expressed on EFT cells (17, 28, 33). Using the combinations of these antibodies listed in Table 2, which are useful for the immunodetection of either MPCs or EFT cells, we further examined whether EWS/ETS expression affects the immunophenotype of UET-13 cells and compared its effect with that on the immunophenotype of EFT cell lines (Table 2 and Fig. 5). As shown in Table 2, UET-13 cells express most of the human primary MPCs markers. Some of the antigens expressed in MPCs, namely, CD29, CD59, CD90, CD105, and CD166, were also found to be expressed in EFT cell lines, but others, namely, CD10, CD13, CD44, CD61, and CD73, were not. In contrast, antigens recognized to be present in EFT cells, including CD40, CD56, and CD133, were absent from UET-13 cells. Interestingly, when the effect of tetracycline-mediated EWS/ETS expression on the immunophenotype of UET-13 cells was tested, levels of some of the antigens present in UET-13 cells, such as CD10, CD13, and CD61, were found to be decreased (Fig. 5). In contrast, some of the markers found in EFT cells, i.e., CD54, CD117, and CD271, became positive in UET-13TR-EWS/ETS cells after tetracycline treatment. Because UET-13TR cells did not show such immunophenotypic change upon treatment with tetracycline, these results indicated that, at least in part, the immunophenotype of UET-13 cells was changed in favor of EFT in the presence of EWS/ETS.

EWS/ETS in UET-13 cells modulates EFT-like gene expression. To further examine the molecular mechanism of EWS/ETS-dependent cellular modulation in human mesenchymal progenitor background, we performed DNA microarray-based expression profiling using the Affymetrix human genome U133 Plus 2.0 array. As a first step to this approach, we validated our experimental systems by analyzing the sequential changes of known EWS/ETS target genes, i.e., inhibitor of differentiation 2 (ID2) (14, 39), NK2 transcription factor related, locus 2 (NKX2.2) (9, 48), and insulin-like growth factor binding protein 3 (IGFBP3) (41). Consistent with previous reports, levels of ID2 and NKX2.2 increased with the expression of EWS/ETS in a time-dependent manner, whereas the expression level of IGFBP3 decreased (Fig. 6A). Employing the same procedure, we also examined whether the change of surface antigen expression was regulated at the transcriptional level and determined the mRNA expression levels of some surface antigens in UET-13 transfectants with or without tetracycline treatment. In accordance with the results of immunocytometric and immunohistological experiments, the mRNA expression levels of CD10, CD13, CD49e, and CD61 were decreased, while those of CD54, CD99, CD117, and CD271 were markedly increased in tetracycline-treated UET-13TR-EWS/ETS cells (Fig. 6B and C), indicating that the expression of these antigens is

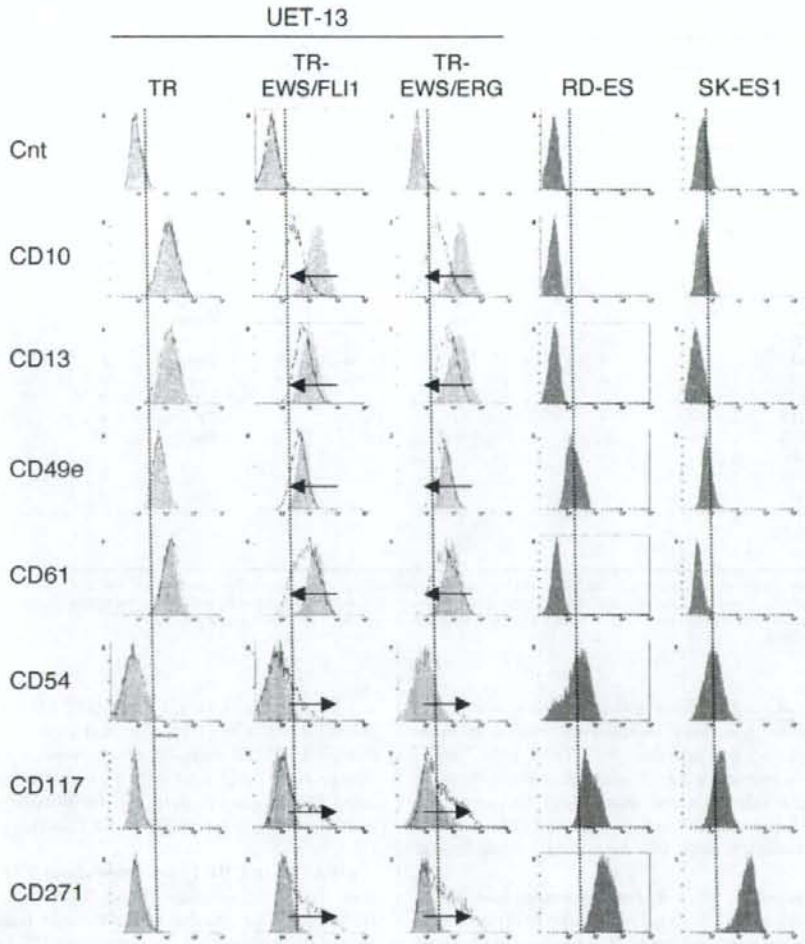

FIG. 5. Immunophenotypic change on induction of EWS/ETS expression in UET-13 cells. UET-13 transfectants were cultured with or without 3 μg/ml of tetracycline for 1 week and flow cytometric analyses were performed by using a set of antibodies as indicated. The histograms of UET-13 transfectants with (empty) and without (gray) tetracycline treatment were overlaid. Dotted lines indicate fluorescence intensities in negative control panels (Cnt). Arrows indicate the immunophenotypic change caused by tetracycline. The immunophenotypes of the EFT cell lines RD-ES and SK-ES1 were also examined.

controlled at the transcriptional level in the presence of EWS/ETS.

We next investigated the candidate genes whose expression is regulated by EWS/ETS in human MPCs. First, we selected the genes with up-regulated or down-regulated expression by EWS/ETS induction using gene cluster analysis (Fig. 7A; UET-13TR-EWS/FLI1 up, 4,294 probes; down, 4,103 probes; UET-13TR-EWS/ERG up, 3,358 probes; down, 3,705 probes). To reduce the number of the candidate genes, we selected up-regulated genes that are expressed in tetracycline-treated cells at least 1.5-fold higher than in untreated cells (UET-13TR-EWS/FLI1, 1,137 probes; UET-13TR-EWS/ERG, 835 probes). Similarly, the down-regulated genes that are expressed in tetracycline-treated cells at least 0.75-fold lower than in untreated cells (UET-13TR-EWS/FLI1, 1,803 probes; UET-13TR-EWS/ERG, 773 probes). By selecting common probes in both cells, we finally identified a group of candidate genes significantly controlled by EWS/ETS induction in the human mesenchymal progenitor background. Since microarray analysis was performed as a global screening in a single experiment, it is likely that there is a fair bit of noise in the derived gene profiles due to the lack of replicate data. This may account in part for the limited overlap between the profiles induced by EWS-FLI1 and EWS-ERG, whereas we still identified 349 probes of common up-regulated genes and 293 probes of common down-regulated genes (see the supplemental material). In addition to the EFT-specific genes mentioned above, these contained those previously described as EFT-specific genes, such as those for OB-cadherin/cadherin-11 (31), Janus

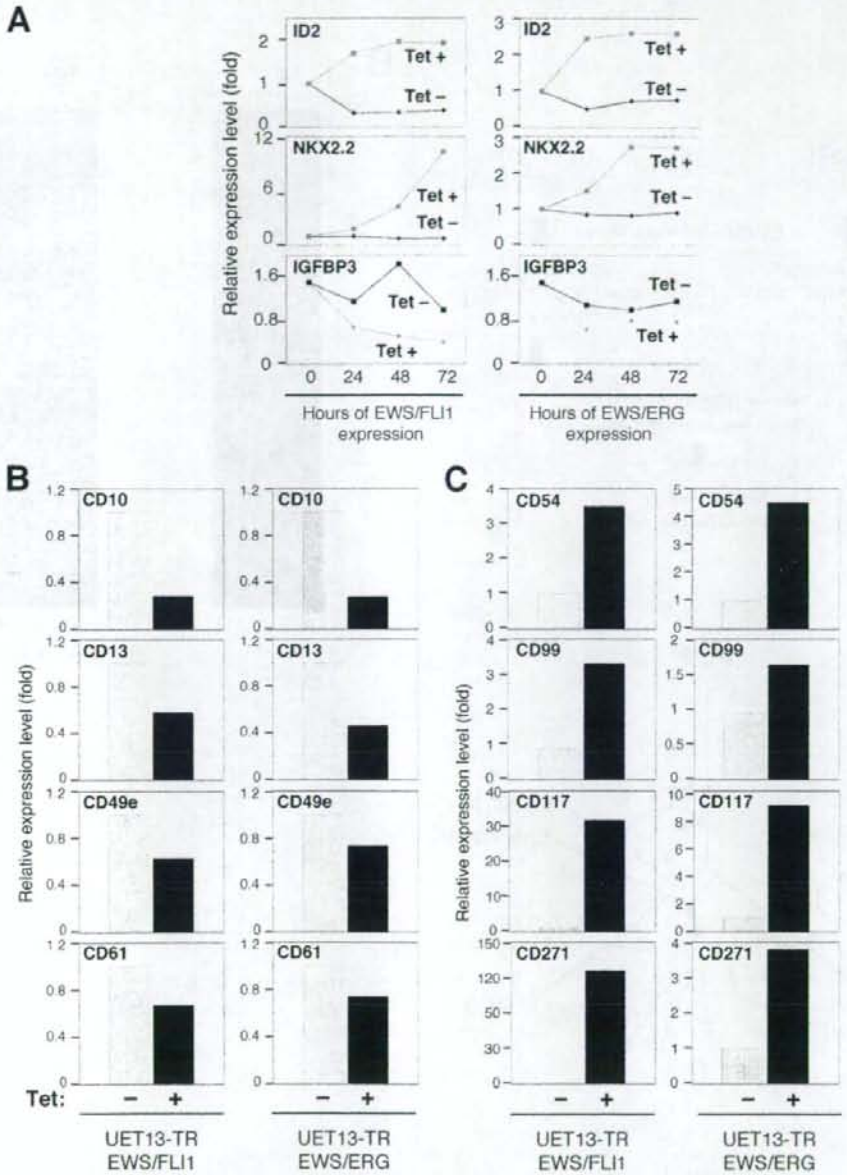

FIG. 6. The change of expression profile on induction of EWS/ETS in UET-13 cells. UET-13TR-EWS/FLI1 and UET-13TR-EWS/ERG cells were cultured in the absence or presence of tetracycline (Tet) for the indicated periods and analyzed using the Affymetrix human genome U133 Plus 2.0 array as described in Materials and Methods. (A) The sequential changes of ID2, NKX2.2, and IGFBP3 mRNA levels in UET-13 transfectants upon treatment with or without tetracycline. Diamond symbols indicate UET-13 transfectants in the absence of tetracycline; box symbols indicate UET-13 transfectants in the presence of tetracycline. (B and C) Microarray studies for the determination of expression profiles of surface antigens in UET-13 transfectants. UET-13 transfectants were treated with or without 3 μg/ml of tetracycline for 72 h. mRNA levels were determined with the Affymetrix human genome U133 Plus 2.0 array.

kinase 1 (JAK1) (49), keratin 18, and six-transmembrane epithelial antigen of the prostate (STEAP) (22). The expression pattern of these genes (642 probes) in UET-13 transfectants in the absence or presence of tetracycline is shown in the gene cluster in Fig. 7B. The expression of these genes was indeed changed significantly after EWS/ETS expression in both cells. They included genes associated with signal transduction (such as those for epidermal growth factor receptor, FAS [CD95], and fibroblast

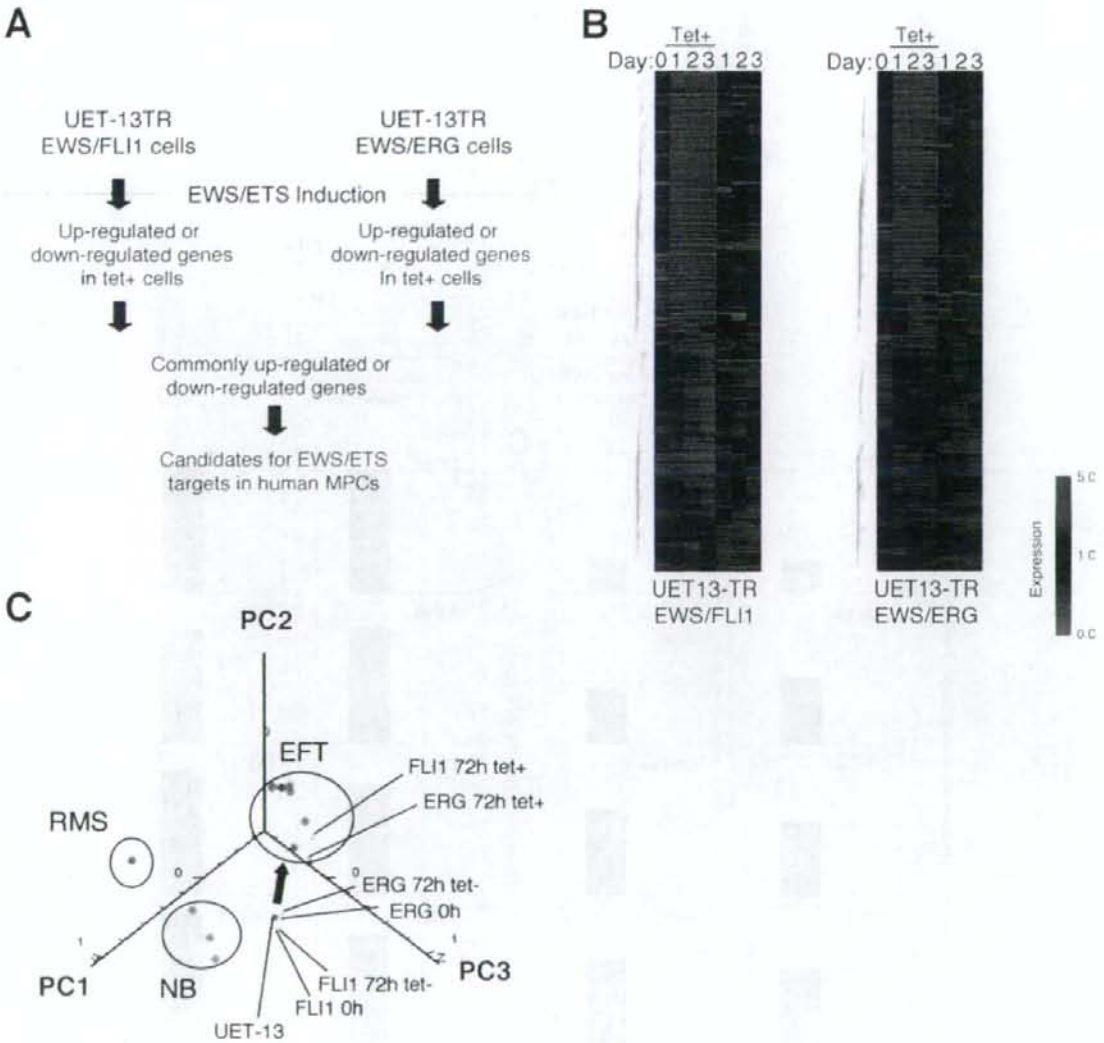

FIG. 7. Identification of candidates for the target of EWS/ETS in human MPCs by use of a microarray. UET-13TR-EWS/FLI1 and UET-13TR-EWS/ERG cells were cultured as described for Fig. 6 and analyzed using the Affymetrix human genome U133 Plus 2.0 array as described in Materials and Methods. (A) Scheme for the analysis of microarray data. (B) Gene cluster analysis of UET-13 transfectants in the absence or presence of tetracycline by use of 642 candidate genes for targets of EWS/ETS in human MPCs. (C) Visualization of sequential change by the gene expression profile in UET-13 transfectants following tetracycline-mediated EWS/ETS expression based on a PCA of 642 candidate genes. Deep blue plots indicate UET-13 cells. Light blue plots indicate UET-13 transfectants in the absence of tetracycline for 72 h. Yellow plots indicate UET-13 transfectants in the presence of tetracycline for 72 h. The pink circle indicates EFT cell lines expressing EWS/FLI1 (purple plots), EWS/ERG (red plot), and EWS/E1AF (light green plot). The light blue circle with blue plots indicates NB cell lines. The yellow circle with an orange plot indicates a rhabdomyosarcoma (RMS) cell line. Cutoff induction and repression levels are 1.5-fold and 0.75-fold, respectively. Tet, tetracycline.